Supporting Information

$Ca_3(TeO_3)_2(MO_4)$ (M = Mo, W): Mid-Infrared Nonlinear Optical Tellurates with Ultrawide Transparency Ranges and Superhigh Laser-Induced Damage Thresholds

Qian Wu[†,§], Jingfang Zhou[†,‡,§], Xiaomeng Liu[†,‡], Xingxing Jiang[†], Qiaoxin Zhang[†,‡], Zheshuai Lin[†], and Mingjun Xia[*,†,‡]

[†]Beijing Center for Crystal Research and Development, Key Laboratory of Functional Crystals and Laser Technology, Technical Institute of Physics and Chemistry, Chinese Academy of Sciences, Beijing 100190, China

[‡]Center of Materials Science and Optoelectronics Engineering, University of Chinese Academy of Sciences, Beijing 100049, China

Corresponding author: xiamingjun@mail.ipc.ac.cn

Table S1. Elemental analysis of Ca, Te, Mo and O in $Ca_3(TeO_3)_2(MoO_4)$ by energy-dispersive X-ray spectroscopy (EDS).

Element	Weight%	Atomic%	Atomic ratio
O K	38.33	75.45	19.86
Ca K	15.21	11.95	3.14
Te L	32.56	8.04	2.12
Mo L	13.90	4.56	1.20
Totals	100.00		

Table S2. Elemental analysis of Ca, Te, W and O in $Ca_3(TeO_3)_2(WO_4)$ by EDS.

Element	Weight%	Atomic%	Atomic ratio
O K	39.73	80.34	26.78
Ca K	11.25	9.08	3.03
Te L	25.15	6.38	2.12
W M	23.88	4.20	1.4
Totals	100.00		

Table S3. Atomic coordinates ($\times 10^4$) and equivalent isotropic displacement parameters ($\times 10^2$) for $Ca_3(TeO_3)_2(MoO_4)$. U_{eq} is defined as one third of the trace of the orthogonalized U_{ij} tensor.

Atom	x	y	z	U(eq)
Ca(1)	71(1)	2784(3)	6321(1)	11(1)
Ca(2)	3152(1)	7563(3)	6983(1)	11(1)
Ca(3)	383(1)	7227(3)	8912(1)	11(1)
Te(1)	2843(1)	2436(1)	9332(1)	9(1)
Te(2)	2599(1)	2686(1)	4518(1)	9(1)
Mo(1)	6472(1)	2576(1)	7815(1)	9(1)
O(1)	1540(5)	5030(8)	5180(4)	11(1)
O(2)	5212(5)	4763(9)	6859(4)	20(1)
O(3)	1668(5)	245(7)	8122(4)	13(1)
O(4)	2169(6)	332(8)	5522(4)	17(1)
O(5)	2382(6)	4916(9)	8165(4)	16(1)
O(6)	1210(5)	3521(7)	9951(4)	15(1)
O(7)	894(5)	1615(8)	3151(4)	20(1)
O(8)	7879(5)	1506(8)	7102(4)	19(1)
O(9)	5230(5)	219(8)	8017(4)	22(1)
O(10)	7508(6)	3819(8)	9290(4)	21(1)

Table S4. Selected bond lengths (Å) and angles (degree) for $Ca_3(TeO_3)_2(MoO_4)$.

Ca(1)-O(1)	2.385(5)	Te(1)-O(6)	1.851(4)
Ca(1)-O(1)	2.418(4)	Te(1)-O(5)	1.872(4)
Ca(1)-O(8)	2.419(4)	Te(1)-O(3)	1.877(4)
Ca(1)-O(7)	2.449(5)	Te(2)-O(4)	1.852(4)
Ca(1)-O(3)	2.504(4)	Te(2)-O(7)	1.855(4)
Ca(1)-O(4)	2.638(5)	Te(2)-O(1)	1.882(4)
Ca(1)-O(5)	2.659(5)	Mo(1)-O(8)	1.751(4)
Ca(1)-O(4)	2.744(5)	Mo(1)-O(9)	1.760(4)
Ca(2)-O(4)	2.229(5)	Mo(1)-O(10)	1.761(4)
Ca(2)-O(5)	2.231(5)	Mo(1)-O(2)	1.763(5)
Ca(2)-O(9)	2.335(5)	O(6)-Te(1)-O(5)	89.97(18)
Ca(2)-O(2)	2.402(5)	O(6)-Te(1)-O(3)	101.20(19)
Ca(2)-O(1)	2.508(5)	O(5)-Te(1)-O(3)	92.07(18)
Ca(2)-O(3)	2.561(4)	O(4)-Te(2)-O(7)	90.95(19)
Ca(3)-O(7)	2.258(4)	O(4)-Te(2)-O(1)	92.76(17)
Ca(3)-O(6)	2.264(4)	O(8)-Mo(1)-O(9)	109.3(2)
Ca(3)-O(3)	2.347(4)	O(8)-Mo(1)-O(10)	110.7(2)
Ca(3)-O(6)	2.388(4)	O(9)-Mo(1)-O(10)	108.9(2)
Ca(3)-O(10)	2.419(5)	O(8)-Mo(1)-O(2)	109.80(19)
Ca(3)-O(5)	2.497(4)		

Table S5. Atomic coordinates ($\times 10^4$) and equivalent isotropic displacement parameters ($\times 10^2$) for $Ca_3(TeO_3)_2(WO_4)$. U_{eq} is defined as one third of the trace of the orthogonalized U_{ij} tensor.

Atom	x	y	z	U(eq)
Ca(1)	8152(3)	3625(6)	6983(2)	11(1)
Ca(2)	5382(3)	3953(5)	89097(18)	10(1)
Ca(3)	5064(3)	8393(6)	63199(19)	10(1)
Te(1)	7831(8)	8746(2)	9328(6)	8(2)
Te(2)	7598(8)	8508(29)	4522(6)	9(2)
W(1)	14699(5)	86117(8)	78143(3)	10(1)
O(1)	6220(12)	7626(13)	9968(8)	17(2)
O(2)	2864(13)	9674(16)	7100(9)	20(1)
O(3)	6524(11)	6182(13)	5180(8)	11(2)
O(4)	7146(13)	10895(15)	0.5512(8)	16(2)
O(5)	7388(12)	0.6254(15)	8169(8)	15(2)
O(6)	6668(12)	10918(14)	8121(8)	11(2)
O(7)	211(12)	6393(14)	6868(8)	20(2)
O(8)	5938(12)	5938(12)	3155(7)	19(2)
O(9)	202(11)	10981(15)	8023(8)	21(2)
O(10)	2518(12)	7371(15)	9291(8)	20(2)

Table S6. Selected bond lengths (Å) and angles (degree) for $Ca_3(TeO_3)_2(WO_4)$.

Ca(1)-O(4)	2.225(9)	Te(1)-O(1)	1.859(9)
Ca(1)-O(5)	2.228(9)	Te(1)-O(6)	1.867(8)
Ca(1)-O(9)	2.322(9)	Te(1)-O(5)	1.872(8)
Ca(1)-O(7)	2.392(10)	Te(2)-O(8)	1.838(9)
Ca(1)-O(3)	2.521(9)	Te(2)-O(4)	1.864(9)
Ca(1)-O(6)	2.573(9)	Te(2)-O(3)	1.884(8)
Ca(2)-O(8)	2.268(8)	W(1)-O(2)	1.745(9)
Ca(2)-O(1)	2.267(9)	W(1)-O(10)	1.764(8)
Ca(2)-O(6)	2.357(9)	W(1)-O(7)	1.772(9)
Ca(2)-O(1)	2.385(9)	W(1)-O(9)	1.785(8)
Ca(2)-O(10)	2.416(9)	O(1)-Te(1)-O(6)	102.2(4)
Ca(2)-O(5)	2.499(9)	O(1)-Te(1)-O(5)	90.1(4)
Ca(3)-O(3)	2.394(9)	O(6)-Te(1)-O(5)	92.4(4)
Ca(3)-O(3)	2.404(9)	O(8)-Te(2)-O(4)	102.3(4)
Ca(3)-O(2)	2.429(10)	O(8)-Te(2)-O(3)	92.8(3)
Ca(3)-O(8)	2.455(9)	O(2)-W(1)-O(10)	110.5(5)
Ca(3)-O(6)	2.503(9)	O(2)-W(1)-O(7)	110.1(4)
Ca(3)-O(4)	2.652(10)	O(10)-W(1)-O(7)	108.5(4)
Ca(3)-O(5)	2.673(10)	O(2)-W(1)-O(9)	109.8(4)
Ca(3)-O(4)	2.714(10)		

Table S7. Structural information and transmission ranges of representative tellurate NLO crystals.

Compound	Space group	Transmission range (μm)
α-$BaTeMo_2O_9$[1]	$Pca2_1$	0.38~5.53
β-$BaTeMo_2O_9$[2]	$P2_1$	0.5~5.0
$BaTeW_2O_9$[3]	$P2_1$	0.4~4.5
$Cs_2TeMo_3O_{12}$[4]	$P6_3$	0.43~5.38
$Cs_2TeW_3O_{12}$[5]	$P6_3$	0.43~5.0
$MgTeMoO_6$[6]	$P2_12_12$	0.36~5.2
$CdTeMoO_6$[7]	$P\bar{4}2_1m$	0.35~5.4
$MnTeMoO_6$[8]	$P2_12_12$	0.41~5.4
$ZnTeMoO_6$[9]	$P2_12_12$	0.35~5.4
Zn_2TeMoO_7[10]	$P2_1$	0.3~5.75
$Na_2TeW_2O_9$[11]	Ia	0.36~5.0
$Na_2Te_3Mo_3O_{16}$[12]	$I2$	0.42~5.4
$Ca_3(TeO_3)_2(MoO_4)$ (this work)	**$P2_1$**	**0.28~5.78**
$Ca_3(TeO_3)_2(WO_4)$ (this work)	**$P2_1$**	**0.29~5.62**

Table S8. Performance comparison of representative MIR NLO crystals.

Compound	Space group	E_g (eV)	Transmission range (μm)	LIDT (MW/cm^2)
$AgGaS_2$[13]	$I\bar{4}2d$	2.75	0.47-13.0	30 (1064nm, 12ns)
$AgGaSe_2$[13]	$I\bar{4}2d$	1.65	0.71-19.0	11 (1064nm, 35ns)
$ZnGeP_2$[14]	$I\bar{4}2d$	2.0	0.74-12	74 (1064nm, 10ns)
$LiInS_2$[14]	$I\bar{4}2d$	3.56	0.34-13.2	100 (1064nm, 10ns)
$BaGa_4S_7$[15]	$Pmn2_1$	3.54	0.35-13.7	80 (1064nm, 15ns)
$BaGa_4Se_7$[16]	Pc	2.64	0.47-18.0	557 (1064nm, 5ns)
$Pb_{17}O_8Cl_{13}$	$Fmm2$	3.44	0.34-13.9	408 (1064nm, 10ns)
KTP[17]	$Pna2_1$	3.5	0.35-4.5	500 (1064nm, 10ns)
KTA[18]	$Pna2_1$	3.6	0.35-5.3	1200 (1064nm, 8ns)
RTP[19]	$Pna2_1$	3.47	0.35-4.5	1800 (1064nm, 10ns)
$La_3SnGa_5O_{14}$[20]	$P321$	4.59	0.27-11	846 (1064nm, 14ns)
Li_2ZrTeO_6[21]	$R3$	4.06	0.29-7.4	1300 (1064nm, 10ns)
$Cs_2TeW_3O_{12}$[5]	$P6_3$	2.89	0.41-5.4	78.1 (1064nm, 10ns)
$BaTeMo_2O_9$[2]	$P2_1$	2.95	0.5-5.0	544 (1064nm, 15ns)
$Ca_3(TeO_3)_2(MoO_4)$	**$P2_1$**	**4.44**	**0.28-5.78**	**1630 (1064nm, 5ns)**
$Ca_3(TeO_3)_2(WO_4)$	**$P2_1$**	**4.27**	**0.29-5.62**	**1500 (1064nm, 5ns)**

Table S9. The directions and magnitudes of the dipole moment of the α-$BaTeMo_2O_9$, β-$BaTeMo_2O_9$, $Cs_2TeMo_3O_{12}$, and $Ca_3(TeO_3)_2(MO_4)$ (M = Mo, W) crystals.

Compound	Species	Dipole moment				
					Magnitude	
		x(*a*)	*y*(*b*)	*z*(*c*)	Debye	$\times 10^{-4}$ esu cm $\cdot$Å^{-3}
α-$BaTeMo_2O_9$	MoO_6	-0.6953	6.7558	2.5942	7.2701	390.55
		-2.0139	6.6993	-3.3143	7.7409	415.84
		1.0903	6.2860	-2.7052	6.9297	372.26
		1.9837	7.1244	3.4081	8.1429	437.44
	TeO_4	2.9017	11.0592	-4.6579	12.3460	663.22
	TeO_3	-2.2219	-9.1377	4.8141	10.5646	567.53
	Unit Cell	0	0	0.556	-	**3.73**
β- $BaTeMo_2O_9$	MoO_6	-2.0442	-0.7697	-5.2901	5.6937	312.39
		5.5516	2.5841	-2.3568	6.5925	361.71
	TeO_4	-9.2109	5.6026	1.3911	10.8889	597.44
	Unit Cell	0	14.834	0	-	**406.95**
$Cs_2TeMo_3O_{12}$	MoO_6	-0.81557	5.102264	-1.64016	5.7922	
	TeO_3	0	0	-7.11467	7.1147	
	Unit Cell	0	0	-17.5097	-	**302.14**
$Ca_3(TeO_3)_2(MoO_4)$ (this work)	MoO_4	0.3132	0.1244	0.0095	0.3371	131.0
	TeO_3	-10.0651	2.9412	-7.4458	13.11	509.0
		-12.5532	-3.0156	1.0308	13.04	507.0
	Unit Cell	0	6.8064	0	-	**269.38**
$Ca_3(TeO_3)_2(WO_4)$ (this work)	WO_4	-0.51397	-0.11901	0.344856	0.63028	242.7
	TeO_3	-13.2705	2.997029	0.763125	13.63	525.0
		-10.6288	-4.30216	-9.36533	14.81	570.0
	Unit Cell	0	-4.31152	0	-	**166.02**

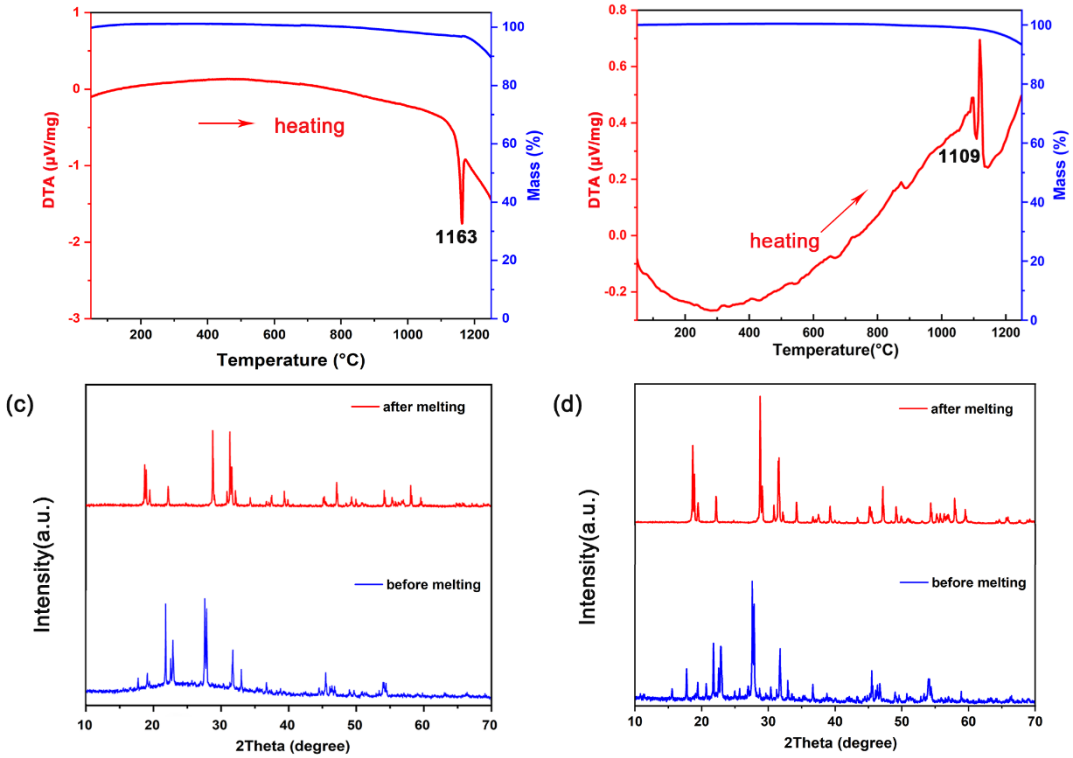

Figure S1. Thermal analysis curves of (a) $Ca_3(TeO_3)_2(MoO_4)$ and (b) $Ca_3(TeO_3)_2(WO_4)$. X-ray diffraction patterns of (c) $Ca_3(TeO_3)_2(MoO_4)$ and (d) $Ca_3(TeO_3)_2(WO_4)$ before and after melting.

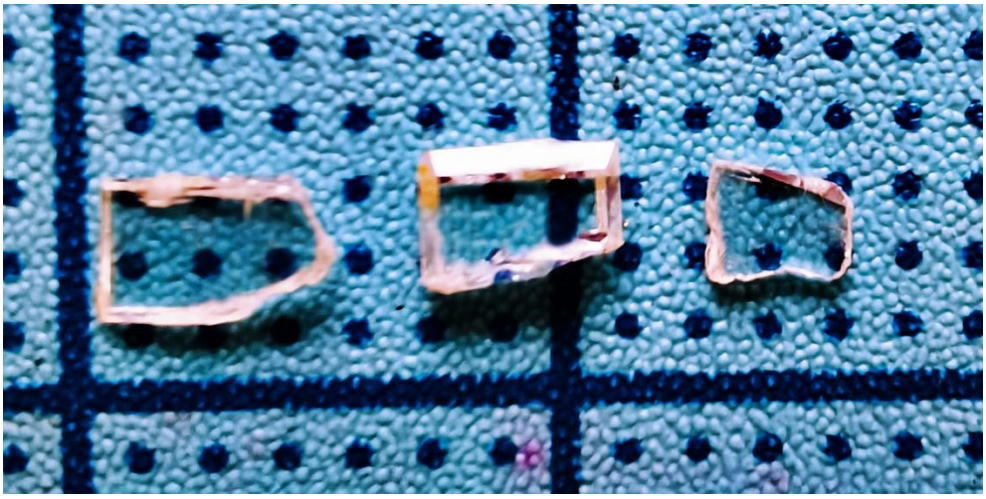

Figure S2. As-grown $Ca_3(TeO_3)_2(MoO_4)$ single crystals.

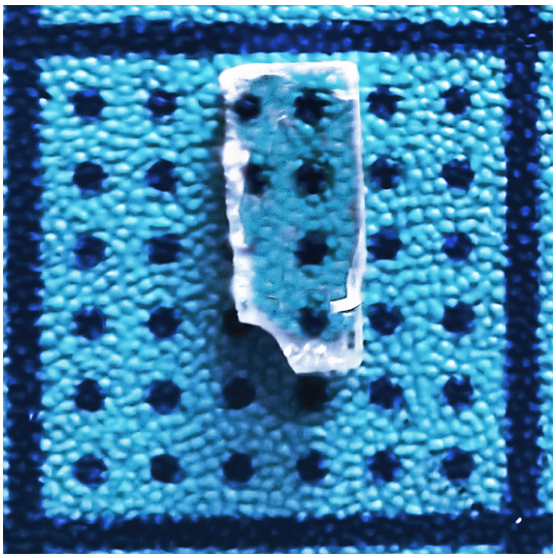

Figure S3. As-grown $Ca_3(TeO_3)_2(WO_4)$ single crystal.

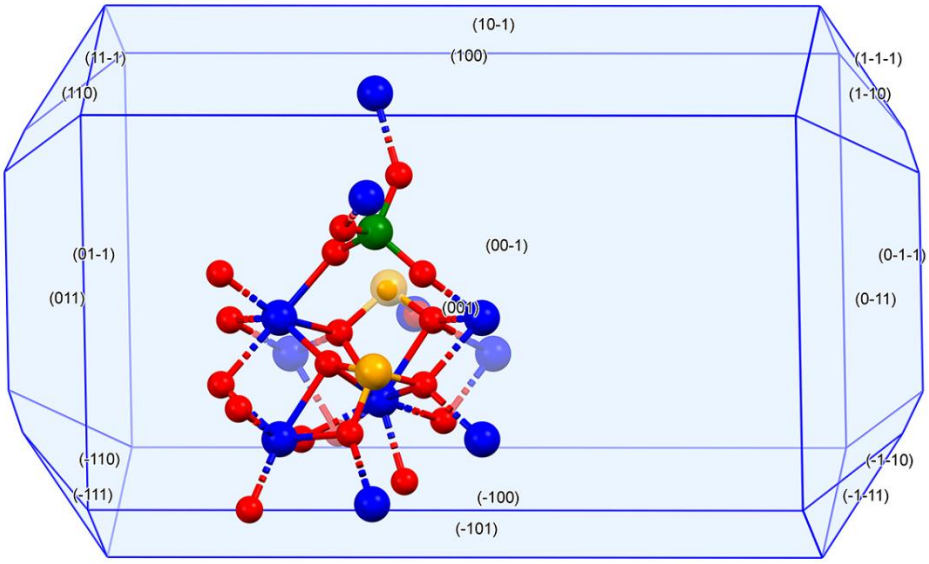

Figure S4. Theoretical morphology of $Ca_3(TeO_3)_2(MoO_4)$ established by the Bravais-Friedel and Donnay-Harker method.

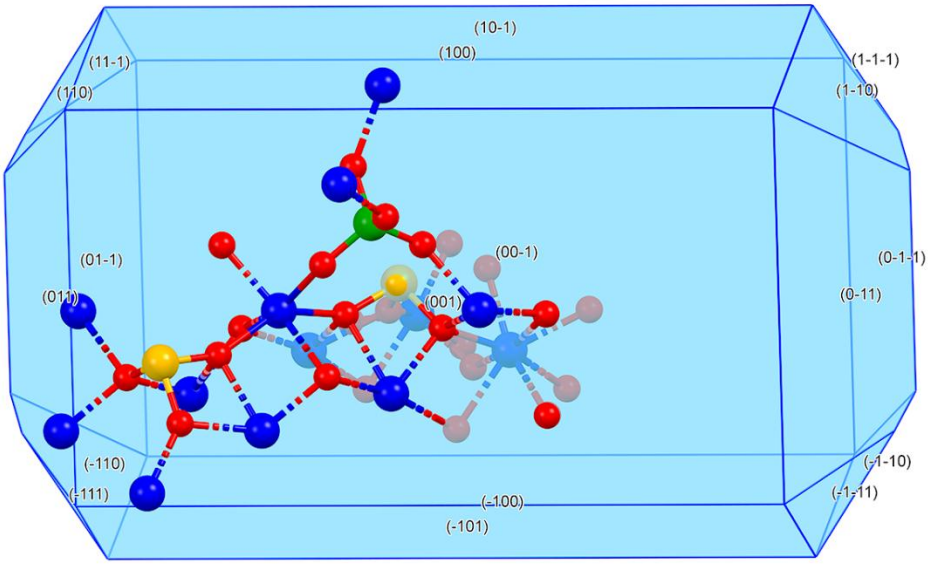

Figure S5. Theoretical morphology of $Ca_3(TeO_3)_2(WO_4)$ established by the Bravais-Friedel and Donnay-Harker method.

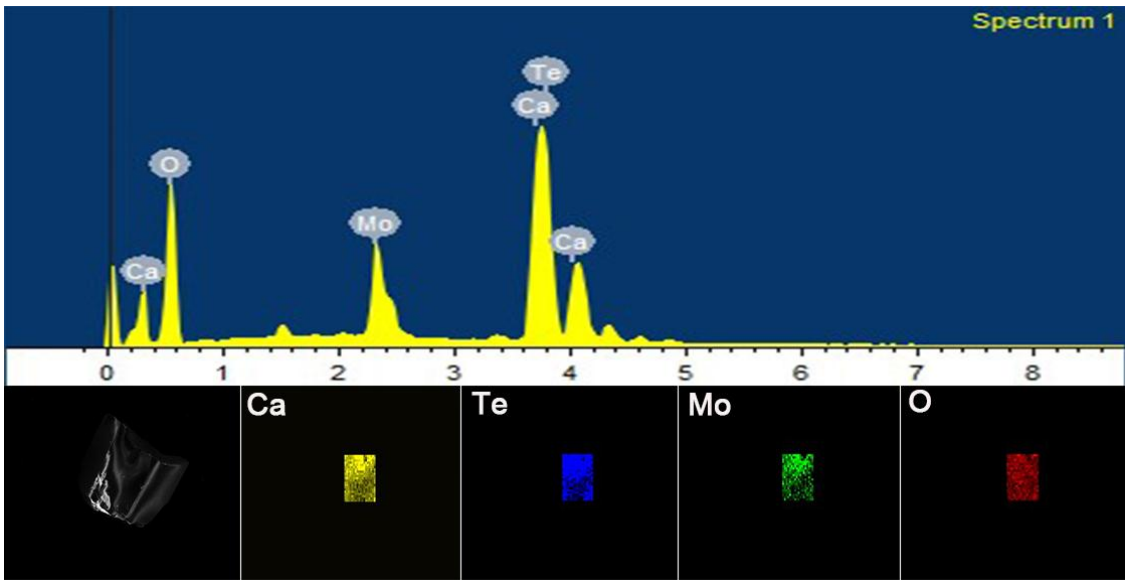

Figure S6. Elemental analysis and mapping images of Ca. Te, Mo, and O elements.

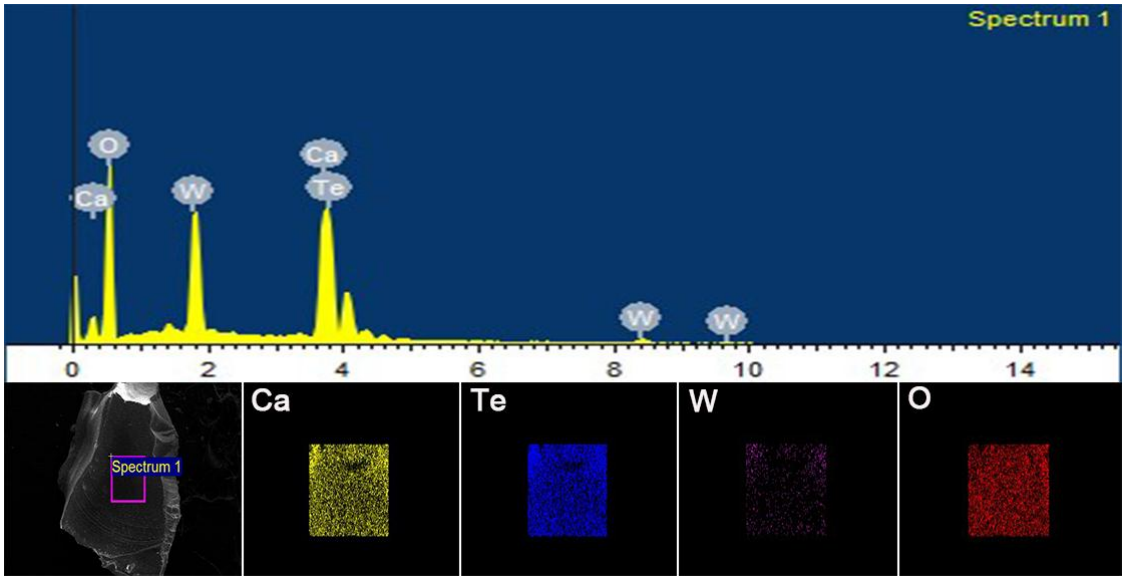

Figure S7. Elemental analysis and mapping images of Ca. Te, W, and O elements.

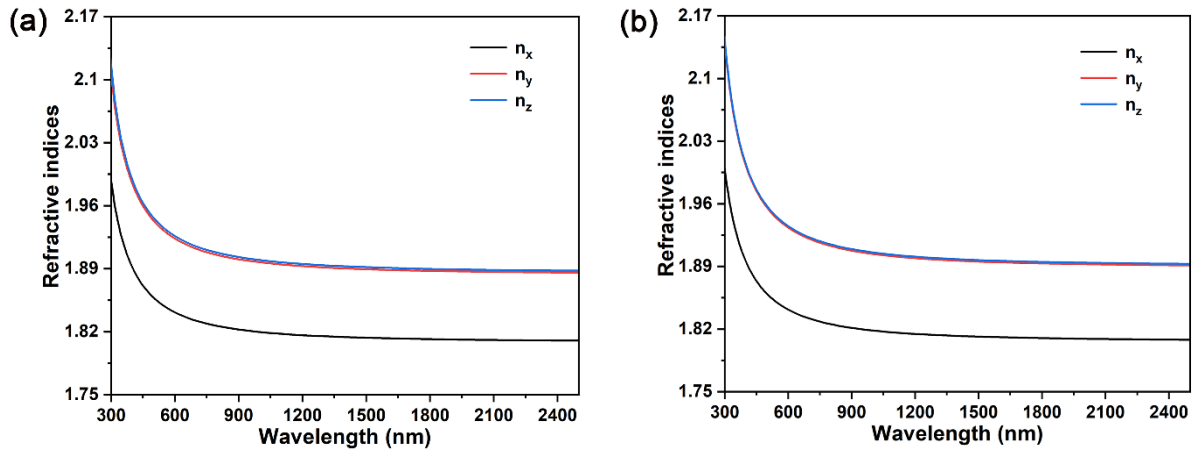

Figure S8. Calculated refractive indices of (a) $Ca_3(TeO_3)_2(MoO_4)$ and (b) $Ca_3(TeO_3)_2(WO_4)$.

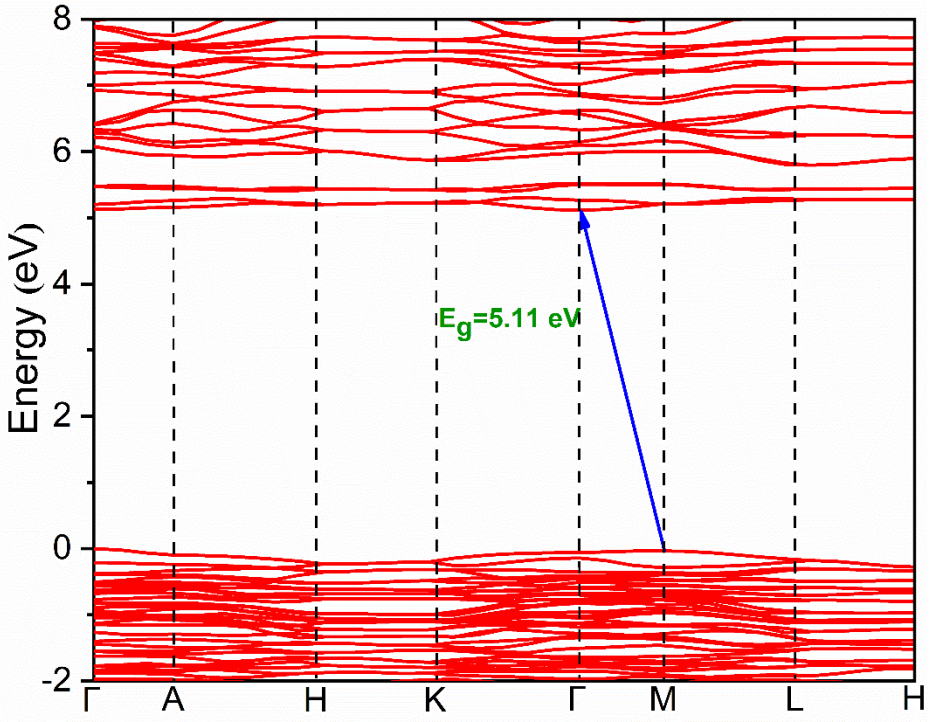

Figure S9. Electronic band structure of $Ca_3(TeO_3)_2(MoO_4)$.

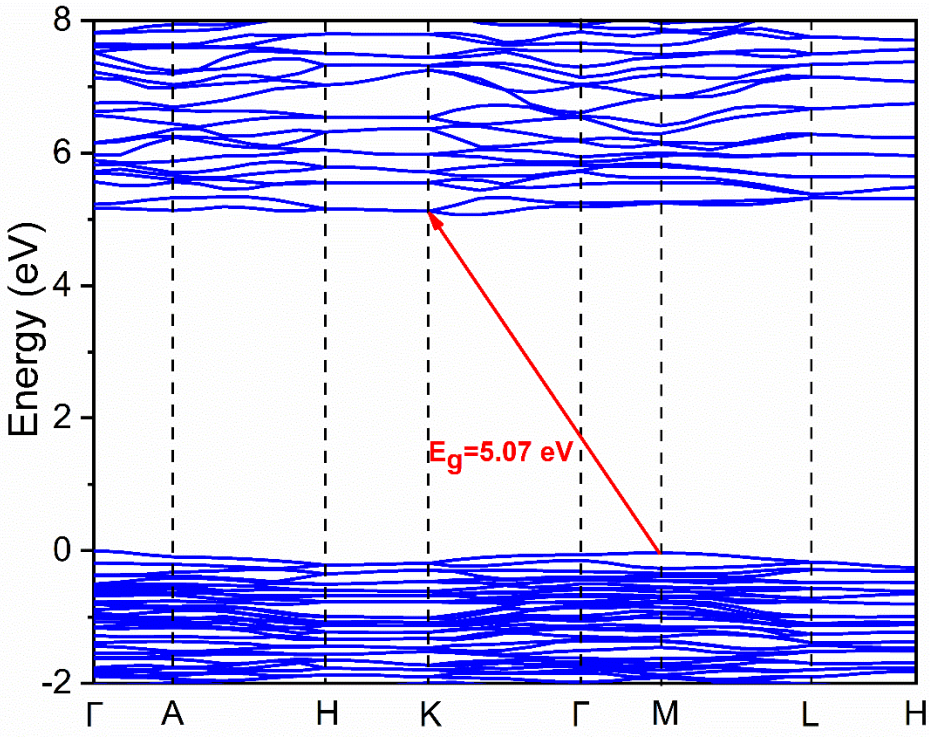

Figure S10. Electronic band structure of $Ca_3(TeO_3)_2(WO_4)$.

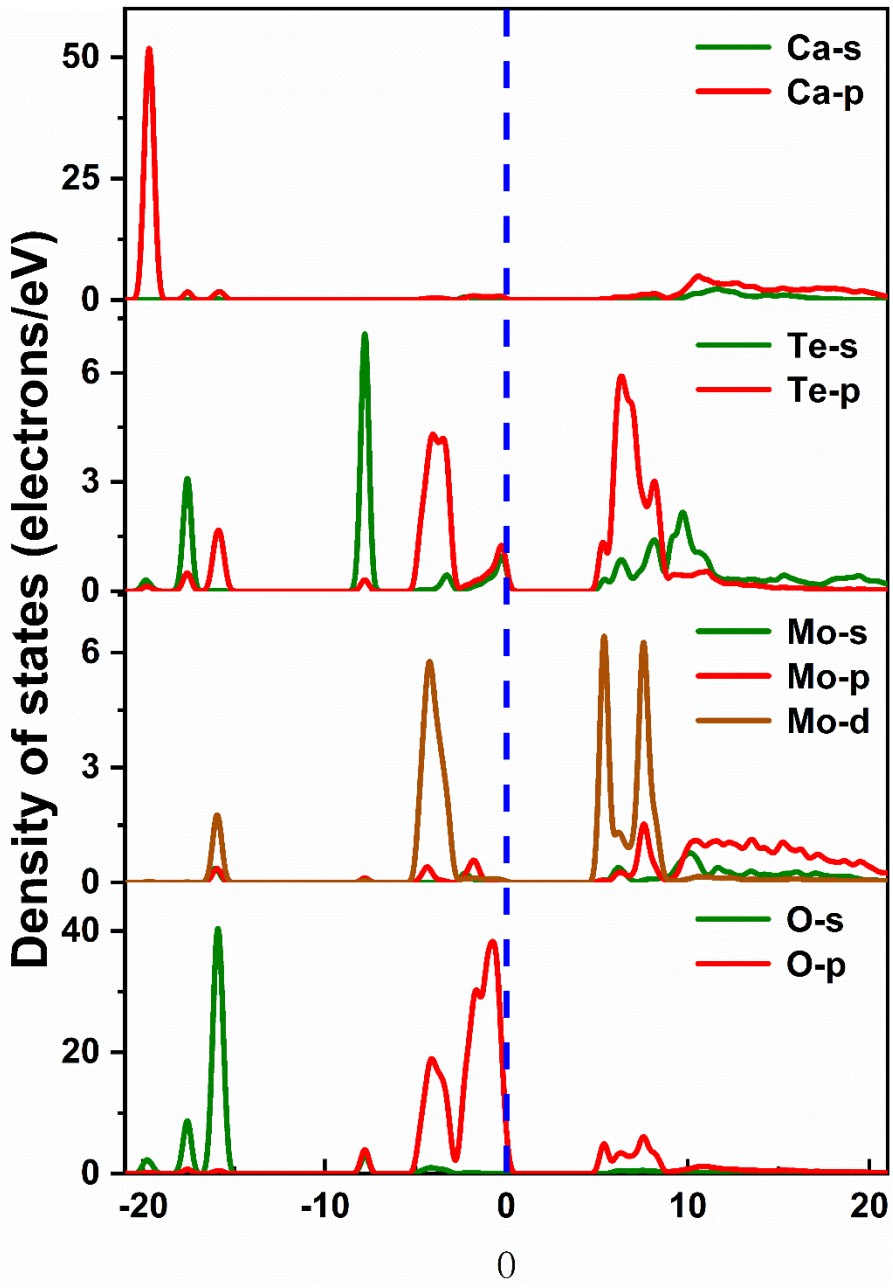

Figure S11. The partial density of states of $Ca_3(TeO_3)_2(MoO_4)$.

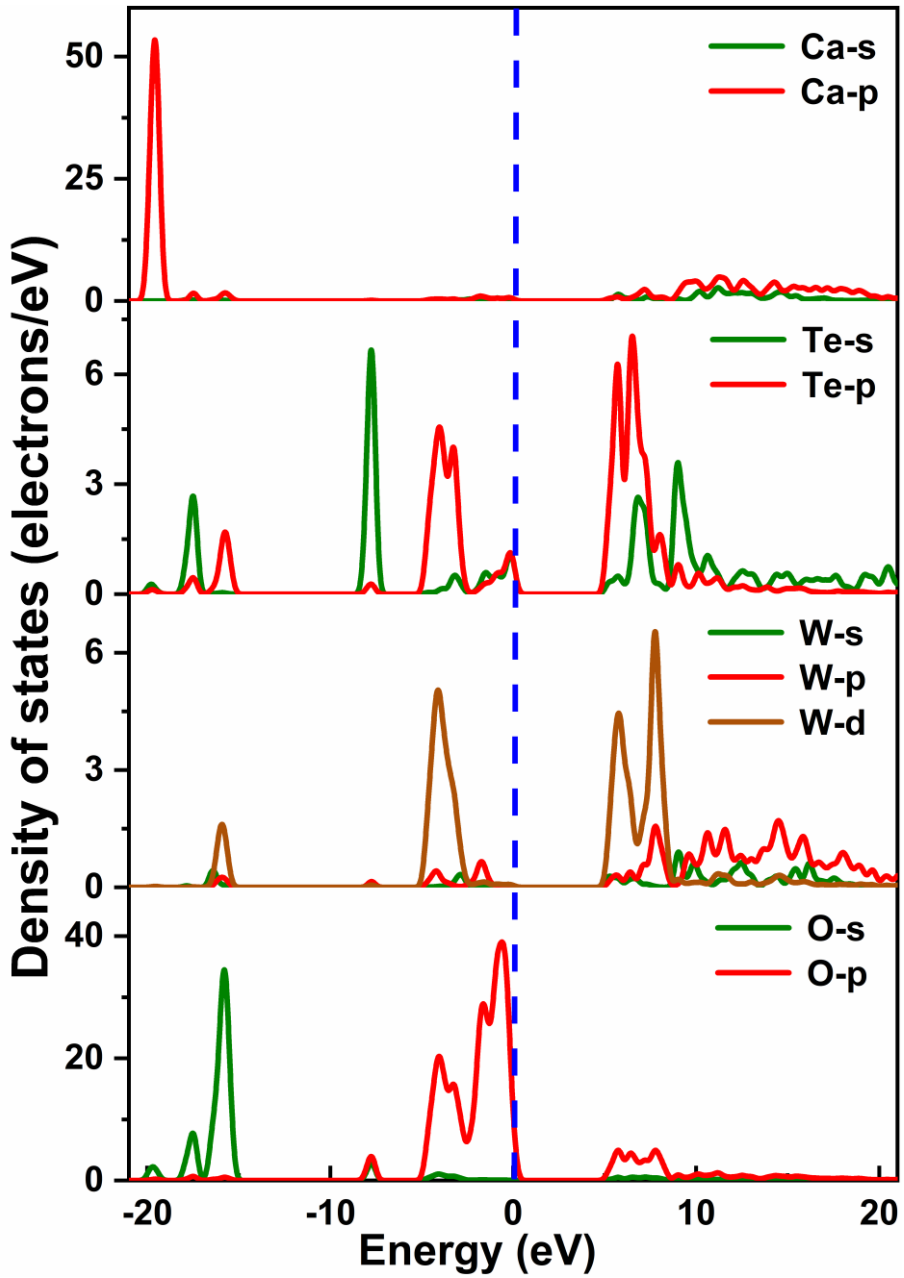

Figure S12. The partial density of states of $Ca_3(TeO_3)_2(WO_4)$.

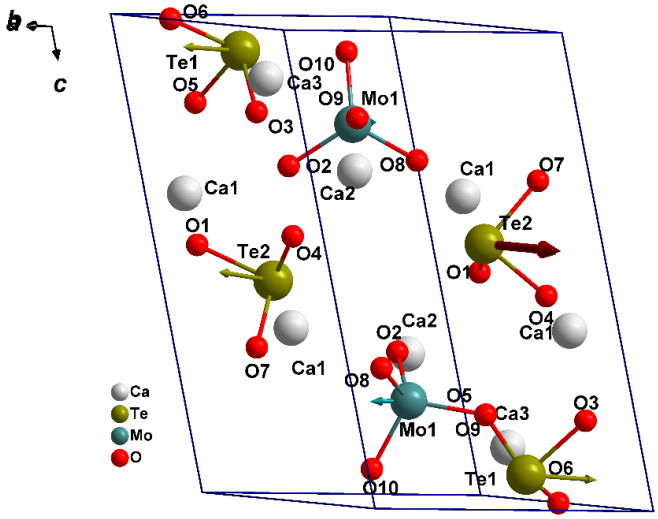

Figure S13. Dipole moment directions of each MoO_4 tetrahedron and TeO_3 trigonal pyramid in $Ca_3(TeO_3)_2(MoO_4)$. The brown arrow indicates the direction of the net dipole moment for the unit cell.

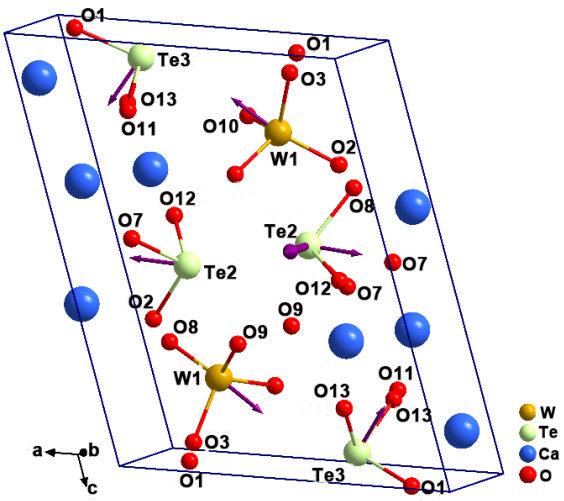

Figure S14. Dipole moment directions of each MoO_4 tetrahedron and TeO_3 trigonal pyramid in $Ca_3(TeO_3)_2(WO_4)$. The purple arrow indicates the direction of the net dipole moment for the unit cell of $Ca_3(TeO_3)_2(WO_4)$.

References

1. Zhang, J. J.; Zhang, Z. H.; Sun, Y. X.; Zhang, C. Q.; Tao, X. T. Bulk crystal growth and characterization of a new polar polymorph of $BaTeMo_2O_9$: α-$BaTeMo_2O_9$. *CrystEngComm*, **2011**, *13*, 6985-6990.

2. Zhang, W. G.; Tao, X. T.; Zhang, C. Q.; Gao, Z. L.; Zhang, Y. Z.; Yu, W. T.; Cheng, X. F.; Liu, X. S.; Jiang, M. H. Bulk Growth and Characterization of a Novel Nonlinear Optical Crystal $BaTeMo_2O_9$. *Cryst. Growth Des.* **2008**, *8*, 304-307.

3. Zhang, Z. H.; Tao, X. T.; Zhang, J. J.; Sun, Y. X.; Zhang, C. Q. ; Li, B. Synthesis, crystal growth, and characterization of the orthorhombic $BaTeW_2O_9$: a new polymorph of $BaTeW_2O_9$. *CrystEngComm*. **2013**, *15*, 10197-10204.

4. Zhang, J. J.; Tao, X. T.; Sun, Y. X.; Zhang, Z. H.; Zhang, C. Q.; Gao, Z. L.; Xia, H. B.; Xia, S. Q. Top-seeded solution growth, morphology, and properties of a polar crystal $Cs_2TeMo_3O_{12}$. *Cryst. Growth Des.* **2011**, *11*, 1863-1868.

5. Zhao, P.; Cong, H. J.; Tian, X. X.; Sun, Y. X.; Zhang, C. Q.; Xia, S. Q.; Gao, Z. L.; Tao, X. T. Top-Seeded Solution Growth, Structure, Morphology, and Functional Properties of a New Polar Crystal-$Cs_2TeW_3O_{12}$. *Cryst. Growth Des.* **2015**, *15*, 4484-4489.

6. Zhang, J. J.; Zhang, Z. H.; Sun, Y. X.; Zhang, C. Q.; Zhang, S. J.; Liu, Y. ; Tao, X. T. $MgTeMoO_6$: A neutral layered material showing strong second-harmonic generation. *J. Mater. Chem.* **2012**, *22*, 9921-9927.

7. Zhao, S. G; Jiang, X. X.; He, R.; Zhang, S. Q.; Sun, Z. H.; Luo, J. H.; Lin, Z. S.; Hong, M. C. A combination of multiple chromophores enhances second-harmonic

generation in a nonpolar noncentrosymmetric oxide: $CdTeMoO_6$. *J. Mater. Chem. C* **2013**, *1*, 2906-2912.

8. Jin, C. G.; Li, Z.; Huang, L. X.; He, M. Z, Top-seeded solution growth and characterization of a novel nonlinear optical crystal $MnTeMoO_6$. *J. Cryst. Growth.* **2013**, *369*, 43-46.

9. Zhao, S. G.; Luo, J. H.; Zhou, P.; Zhang, S. Q.; Sun, Z. H.; Hong, M. C. $ZnTeMoO_6$: a strong second-harmonic generation material originating from three types of asymmetric building units. *RSC Adv.* **2013**, *3*, 14000-14006.

10. Zhang, W. G.; Halasyamani, P. S. Top-seeded solution crystal growth of noncentrosymmetric and polar Zn_2TeMoO_7 (ZTM). *J. Solid State. Chem.* **2016**, *236*, 32-38.

11. Zhang, W. L.; Sun, J. F.; Wang, X. Q.; Shen, G. Q.; Shen, D. Z. Crystal growth and optical properties of a noncentrosymmetric molybdenum tellurite, $Na_2Te_3Mo_3O_{16}$. *CrystEngComm*. **2012**, *14*, 3490-3494.

12. Chi, E. O.; Ok, K. M.; Porter, Y.; Halasyamani, P. S. $Na_2Te_3Mo_3O_{16}$: A New Molybdenum Tellurite with Second‐Harmonic Generating and Pyroelectric Properties. *Chem. Mater.* **2006**, *18*, 2070-2074.

13. Chung, I.; Kanatzidis, M. G. Metal Chalcogenides: A Rich Source of Nonlinear Optical Materials. *Chem. Mater.* **2014**, *26*, 849-869.

14. Becker, P. Borate Materials in Nonlinear Optics. *Adv. Mater.* **1998**, *10*, 979-992.

15. Lin, X.; Zhang, G.; Ye, N. Growth and Characterization of $BaGa_4S_7$: A New Crystal for Mid-IR Nonlinear Optics. *Cryst. Growth Des.* **2009**, *9*, 1186-1189.

16. Yao, J. Y.; Yin, W. L.; Feng, K.; Li, X. M·; Mei, D. J.; Lu, Q. M.; Ni, Y. B.; Zhang, Z. W.; Hu, Z. G.; Wu, Y. C. Growth and characterization of $BaGa_4Se_7$ crystal. *J. Cryst. Growth.* **2012**. *346*, 1-4.

17. Torabi-Goudarzi, F.; Riis, E. Efficient cw high-power frequency doubling in periodically poled KTP. *Opt. Comm.* **2003**, *227*, 389-403.

18. Bosenberg, W. R.; Cheng, L. K.; Bierlein, J. D. Optical parametric frequency conversion properties of $KTiOAsO_4$. *Appl. Phys. Lett.* **1994**, *65*, 2765-2767.

19. Oseledchik, Y. S.; Belokrys, S. P.; Osadchuk, V. V.; Prosvirnin, A. L.; Selevich, A. F.; Starshenko, V. V.; Kuzemchenko, K. V. Growth of $RbTiOPO_4$ single crystals from phosphate systems. *J. Cryst. Growth.* **1992**, *125*, 639-643.

20. Lan, H. C.; Liang, F.; Jiang, X. X.; Zhang, C.; Yu, H. H.; Lin, Z. S.; Zhang, H. J.; Wang, J. Y.; Wu, Y. C. Pushing Nonlinear Optical Oxides into the Mid-Infrared Spectral Region Beyond 10 μm: Design, Synthesis, and Characterization of $La_3SnGa_5O_{14}$. *J. Am. Chem. Soc.* **2018**, *140*, 4684-4690.

21. Lu, W. Q.; Gao, Z. L.; Liu, X. T.; Tian, X. X.; Wu, Q.; Li, C. G.; Sun, Y. X.; Liu, Y.; Tao, X. T. Rational Design of a $LiNbO_3$‑like Nonlinear Optical Crystal, Li_2ZrTeO_6, with High Laser-Damage Threshold and Wide Mid-IR Transparency Window. *J. Am. Chem. Soc.* **2018**, *140*, 13089-13096.